Momentum space design of high-Q photonic crystal optical cavities

Kartik Srinivasan and Oskar Painter

Department of Applied Physics, California Institute of Technology, Pasadena, CA 91125, USA.

kartik@caltech.edu

Abstract: The design of high quality factor (Q) optical cavities in two dimensional photonic crystal (PC) slab waveguides based upon a momentum space picture is presented. The results of a symmetry analysis of defect modes in hexagonal and square host photonic lattices are used to determine cavity geometries that produce modes which by their very symmetry reduce the vertical radiation loss from the PC slab. Further improvements in the Q are achieved through tailoring of the defect geometry in Fourier space to limit coupling between the dominant momentum components of a given defect mode and those momentum components which are either not reflected by the PC mirror or which lie within the radiation cone of the cladding surrounding the PC slab. Numerical investigations using the finite-difference time-domain (FDTD) method predict that radiation losses can be significantly suppressed through these methods, culminating with a graded square lattice design whose total Q approaches 10^5 with a mode volume of approximately 0.25 cubic half-wavelengths in vacuum.

OCIS codes: (230.5750) Resonators; (140.5960) Semiconductor lasers

References and links

1. H. Yokoyama, "Physics and Device Application of Optical Microcavities," Science **256,** 66–70 (1992).
2. J. L. Jewell, J. P. Harbison, A. Scherer, Y. H. Lee, and L. T. Florez, "Vertical-Cavity Surface-Emitting Lasers: Design, Growth, Fabrication, Characterization," IEEE J. Quan. Elec. **27,** 1332–1346 (1991).
3. S. L. McCall, A. F. J. Levi, R. E. Slusher, S. J. Pearton, and R. A. Logan, "Whispering-gallery mode lasers," Appl. Phys. Lett. **60,** 289–291 (1992).
4. S. M. Spillane, T. J. Kippenberg, and K. J. Vahala, "Ultralow-threshold Raman laser using spherical dielectric microcavity," Nature **415,** 621–623 (2002).
5. B. E. Little, S. T. Chu, W. Pan, D. Ripin, T. Kaneko, Y. Kokubun, and E. Ippen, "Vertically Coupled Glass Microring Resonator Channel Dropping Filters," IEEE Photonics Tech. Lett. **11,** 215–217 (1999).
6. S. Noda, A. Chutinan, and M. Imada, "Trapping and emission of photons by a single defect in a photonic bandgap structure," Nature **407,** 608–610 (2000).
7. S. Fan, P. R. Villeneuve, and J. D. Joannopoulos, "Channel drop filters in photonic crystals," Opt. Express **3,** 4–11 (1998), http://www.opticsexpress.org/abstract.cfm?URI=OPEX-3-1-4.
8. G. Khitrova, H. M. Gibbs, F. Jahnke, M. Kira, and S. W. Koch, "Nonlinear optics of normal-mode-coupling semiconductor microcavities," Rev. Mod. Phys. **71,** 1591–1639 (1999).
9. D. M. Atkin, P. S. J. Russell, T. A. Birks, and P. J. Roberts, "Photonic band structure of guided Bloch modes in high index films fully etched through with periodic microstructure," J. Mod. Opt. **43,** 1035–1053 (1996).
10. S. G. Johnson, S. Fan, P. R. Villeneuve, J. D. Joannopoulos, and L. A. Kolodziejaki, "Guided modes in photonic crystal slabs," Phys. Rev. B **60,** 5751–5758 (1999).
11. A. Yariv, Y. Xu, R. K. Lee, and A. Scherer, "Coupled-resonator optical waveguide: a proposal and analysis," Opt. Lett. **24,** 711–713 (1999).

#1301 - $15.00 US Received June 03, 2002; Revised July 17, 2002

12. C. Smith, R. De la Rue, M. Rattier, S. Olivier, H. Benisty, C. Weisbuch, T. Krauss, U. Oesterlé, and R. Houdré, "Coupled guide and cavity in a two-dimensional photonic crystal," Appl. Phys. Lett. **78,** 1487–1489 (2001).
13. O. Painter, K. Srinivasan, J. D. O'Brien, A. Scherer, and P. D. Dapkus, "Tailoring of the resonant mode properties of optical nanocavities in two-dimensional photonic crystal slab waveguides," J. Opt. A **3,** S161–S170 (2001).
14. O. J. Painter, A. Husain, A. Scherer, J. D. O'Brien, I. Kim, and P. D. Dapkus, "Room Temperature Photonic Crystal Defect Lasers at Near-Infrared Wavelengths in InGaAsP," J. Lightwave Tech. **17,** 2082–2088 (1999).
15. O. Painter, J. Vučković, and A. Scherer, "Defect Modes of a Two-Dimensional Photonic Crystal in an Optically Thin Dielectric Slab," J. Opt. Soc. Am. B **16,** 275–285 (1999).
16. J. Vučković, M. Lončar, H. Mabuchi, and A. Scherer, "Design of photonic crystal microcavities for cavity QED," Phys. Rev. E 65 (2002).
17. T. Yoshie, J. Vučković, A. Scherer, H. Chen, and D. Deppe, "High quality two-dimensional photonic crystal slab cavities," Appl. Phys. Lett. **79,** 4289–4291 (2001).
18. O. Painter and K. Srinivasan, "Localized defect states in two-dimensional photonic crystal slab waveguides: a simple model based upon symmetry analysis," submitted to Phys. Rev. B (2002).
19. This can be viewed in the far-field as elimination of lower-order multi-pole radiation components[23].
20. E. Yablonovitch, T. J. Gmitter, R. D. Meade, A. M. Rappe, K. D. Brommer, and J. D. Joannopoulos, "Donor and acceptor modes in photonic band-structure," Phys. Rev. Lett. **67,** 3380–3383 (1991).
21. M. Tinkham, *Group Theory and Quantum Mechanics*, *International Series in Pure and Applied Physics* (McGaw-Hill, Inc., New York, NY, 1964).
22. K. Sakoda, *Optical Properties of Photonic Crystals* (Springer-Verlag, Berlin, Germany, 2001).
23. S. G. Johnson, S. Fan, A. Mekis, and J. D. Joannopoulos, "Multipole-cancellation mechanism for high-Q cavities in the absence of a complete photonic band gap," Appl. Phys. Lett. **78,** 3388–3390 (2001).

1 Introduction

The study of high quality factor (Q) optical microcavities is of significance to both lightwave technology and studies in quantum optics[1]. In the former case, such cavities are integral to the development of low threshold microlasers [2, 3], nonlinear optical elements [4], and narrow linewidth, wavelength selective filters [5, 6, 7]. In the latter area, a microcavity with suitable properties will give rise to a host of possible experiments for studying coherent electron-photon interactions [8] and their potential applications in quantum information processing. Optical cavities formed by localized defects in a periodic dielectric structure, or photonic crystal (PC), offer an appealing architecture for such work. Planar two-dimensional (2D) PC slab waveguides (WGs) have in particular been the subject of much research activity in recent years [9, 10] owing to the maturity of current planar fabrication technology. This has been demonstrated in the ability to integrate PC microresonators with WGs [6, 11, 12], and in defect cavity lasers with prescribed emission properties [13] and modal volumes approaching the theoretical limit of a cubic half-wavelength.

While the PC optical microcavities studied in [14] had very small mode volumes and loss properties sufficient to sustain lasing, the measured Q values were still less than 1500. In particular, the radiation losses were predominantly out-of-plane, while the in-plane losses were in comparison small [15]. Although refinements in design [16] and fabrication [17] have since increased the total measured Q to as high as 2800, most of the potential applications previously mentioned require Q values on the order of 10^4 or 10^5 in order for PC slab WG microcavities to show marked improvement from what is available through non-PC designs.

The limitations on Q stem from a number of possible factors, including intrinsic material absorption, etch-induced surface roughness and surface-state absorption, and other fabrication irregularities that prevent ideal replication of a given design. These issues aside, the fundamental design of these cavities has room for improvement, and

#1301 - $15.00 US Received June 03, 2002; Revised July 17, 2002

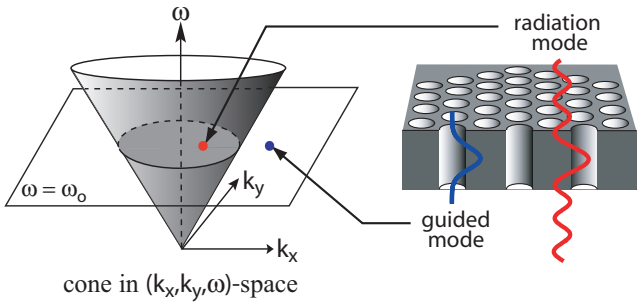

Fig. 1. 2D hexagonal PC slab waveguide structure and cladding light cone.

as such, the focus of this paper primarily lies here. Our main objective is to consider simple design rules that can be used to significantly reduce the vertical losses from such structures, while maintaining or even improving upon the in-plane losses. In Section **2**, we describe a simple picture which illustrates that the vertical radiation loss of a mode is characterized by the presence of momentum components within the light cone of the cladding of the host slab WG. We then consider (Section **3**) the use of symmetry to eliminate in-plane momentum components ($\mathbf{k}_\perp$) at $\mathbf{k}_\perp = 0$ (DC), thereby reducing the vertical loss in the structure. Drawing heavily from [13, 18], we summarize the different defect modes available in hexagonal and square lattice PC's, and proceed to choose target symmetries for modes in these lattices based upon the constraints they impose on the dominant field components of the modes. In Section **4**, we propose simple defect geometries that support such modes and present the results of three dimensional (3D) finite-difference time-domain (FDTD) calculations of their relevant properties. Finally (Section **5**), we consider further improvements in the designs based on a Fourier space tailoring of the defect geometries that reduces coupling of the mode's dominant Fourier components to components that radiate. The results of FDTD simulations of these improved designs in a square lattice are presented, and show that a modal Q-factor approaching 10^5 can be achieved by a careful consideration of the mode and defect geometry in Fourier space.

2 Momentum Space Consideration of Vertical Radiation Loss

The optical cavities studied here are comprised of defects situated in 2D PC slab WGs (Figure 1). As a result, the in-plane confinement of the defect mode is governed by the Distributed Bragg Reflection (DBR) of the surrounding photonic lattice. Leakage of light in the plane of the PC slab WG from the cavity is thus determined by the number of periods of the host lattice surrounding the defect and the width and angular extent of the in-plane guided mode bandgap. The vertical confinement, on the other hand, is due to standard waveguiding by total internal reflection. Vertical radiation loss occurs when the magnitude of the in-plane momentum component, $k_\perp$, is inappropriate to support guiding. More concretely, we note that the energy-momentum dispersion relationship for a homogenous dielectric cladding (refractive index n) of the PC slab WG is $(n\omega/c)^2 = k_\perp^2 + k_z^2$, where ω is the angular frequency, k_z is the momentum normal to the slab, and c is the speed of light. For an air clad PC WG as studied here, $k_\perp^2 = (\omega/c)^2$ defines a cone in (k_x, k_y, ω) space, commonly referred to as the "light cone" (Figure 1). Modes that radiate vertically will have small in-plane momentum components that lie within the light cone of the cladding. This simple rule serves as our fundamental guideline in designing cavities that limit vertical radiation loss. In particular, we seek

#1301 - $15.00 US
Received June 03, 2002; Revised July 17, 2002

out structures that support resonant modes whose in-plane momentum components are primarily situated outside of the cladding light cone.

Before discussing methods to improve the vertical loss properties of PC defect cavities, it is instructive to consider the characteristics of the previously studied[15] dipole-like defect modes in a hexagonal lattice PC. Consider the x-dipole donor mode produced by a symmetric defect consisting of the removal of a single air hole from a hexagonal lattice of air holes in a 2D slab WG[15] (illustrated in cross-section in Figure 1). Following the symmetry analysis presented in reference [13], we see that this mode is composed of dominant Fourier components directed along $\pm\{\mathbf{k}_{X_1}, \mathbf{k}_{X_2}, \mathbf{k}_{X_3}\}$, where the $\mathbf{k}_X$ directions are shown in the hexagonal PC reciprocal space lattice of Figure 2(a). The 2D spatial Fourier Transform (FT) of the x-dipole field component $\mathbf{E}_x$ at the middle of the PC slab WG is given in Figure 3(a). It shows the E-field to be primarily composed of momentum components located about the X points, with $\pm\mathbf{k}_{X_1}$ as the strongest components. Note that the field has a significant number of momentum components lying within the light cone, the boundary of which is shown in Figure 3(a) as a dashed white circle. These low momentum components radiate and are the cause of the mode's relatively low effective vertical Q-factor ($Q_\perp \approx 1000$).

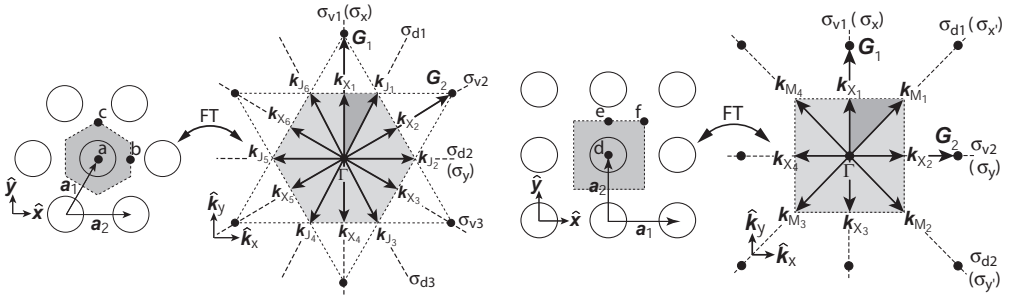

(a) Hexagonal Lattice. (b) Square Lattice.

Fig. 2. Real and reciprocal space lattices of (a) a 2D hexagonal lattice, and (b) a 2D square lattice. For the hexagonal lattice: $|\mathbf{a}_1| = |\mathbf{a}_2| = a$, $|\mathbf{G}_1| = |\mathbf{G}_2| = 4\pi/\sqrt{3}a$, $|\mathbf{k}_X| = 2\pi/\sqrt{3}a$, $|\mathbf{k}_J| = 4\pi/3a$. For the square lattice: $|\mathbf{a}_1| = |\mathbf{a}_2| = a$, $|\mathbf{G}_1| = |\mathbf{G}_2| = 2\pi/a$, $|\mathbf{k}_X| = \pi/a$, $|\mathbf{k}_M| = \sqrt{2}\pi/a$.

3 Symmetry Analysis of Defect Modes in Hexagonal and Square Lattices

There are a number of ways to limit the presence of the small in-plane momentum components in the localized resonant modes of PC slab WG defect cavities. For example, the geometry of the defect and the surrounding holes can be tailored to reduce the magnitude of these components, as was done in [16], where the authors report a predicted Q of $30,000$. One particularly appealing way to limit the presence of small in-plane momentum components is to use symmetry to enforce specific boundary conditions on the Fourier space representation of the mode[19]. A defect will support one or more resonant modes with symmetries that are compatible with the nature of the defect and the surrounding PC. Of particular interest are modes whose symmetry is odd about mirror planes normal to the dominant Fourier components of the mode. In the context of our symmetry analysis (discussed below), the fields of the approximate TE-like modes have in-plane electric field polarization normal to the direction of their dominant Fourier components. Our choice of symmetry minimizes vertical radiation from in-plane electric

#1301 - $15.00 US Received June 03, 2002; Revised July 17, 2002

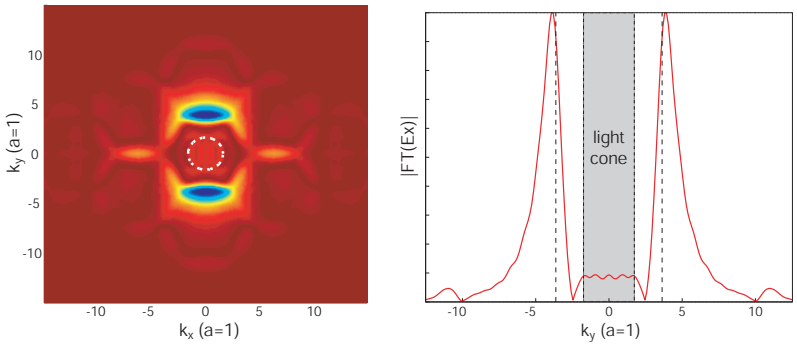

(a) 2D FT of E_x.

(b) 1D FT of E_x along k_y direction.

Fig. 3. Spatial FT of x-dipole donor mode in a hexagonal lattice ($r/a = 0.30$) with a central missing air hole. (a) in 2D, (b) along the k_y direction with $k_x = 0$.

field polarizations parallel to those of the approximate modal fields. In Fourier space this is equivalent to eliminating these in-plane electric field polarizations at $\mathbf{k}_\perp = 0$ (DC). This elimination of DC momentum components is the first step in reducing vertical radiation loss, and serves as our fundamental criterion for choosing the desired symmetry for our defect mode.

The defect modes of a PC cavity are generally classified into donor and acceptor type modes [20], based upon whether the defect creates modes from the conduction band-edge (donor modes) or valence band-edge (acceptor modes). For the hexagonal lattice, whose real and reciprocal space depictions are given in Figure 2(a), the valence band-edge is at the J-point and the conduction band-edge is at the X-point (Figure 4(a)), while the square lattice of Figure 2(b) has its valence band-edge at the M-point and conduction band-edge at the X-point (Figure 4(b)). The dominant Fourier components and symmetry of a defect mode are determined by the type of mode (donor or acceptor) under consideration, the symmetry of the surrounding PC lattice, and the point group symmetry of the defect. The use of such an analysis to produce approximate forms for the modes in hexagonal and square lattice PC defect cavities is the focus of other recent articles [13, 18], and as such, we primarily incorporate the results of these works and describe their implications towards the design of high-Q defect resonators. The course of study is the following: we use the results of [13] and [18] to determine the symmetry and dominant Fourier components for the available donor and acceptor type modes formed at different high symmetry points within hexagonal and square lattice PC's. Candidate modes for high-Q resonators are then chosen from these sets of available modes based upon the criteria placed on the mode's momentum components as described above. Within the mirror plane of the slab WG (coordinates $\mathbf{r}_\perp$) the fundamental even modes are described by the field components $\mathbf{E}_x$, $\mathbf{E}_y$, and $\mathbf{B}_z$. Since the magnetic field is exactly scalar within this mirror plane, the criterion reduces to looking for modes in which the magnetic field pattern is spatially even in the directions of its dominant Fourier components. This is equivalent to having the in-plane electric field components spatially odd in these directions.

#1301 - $15.00 US
Received June 03, 2002; Revised July 17, 2002

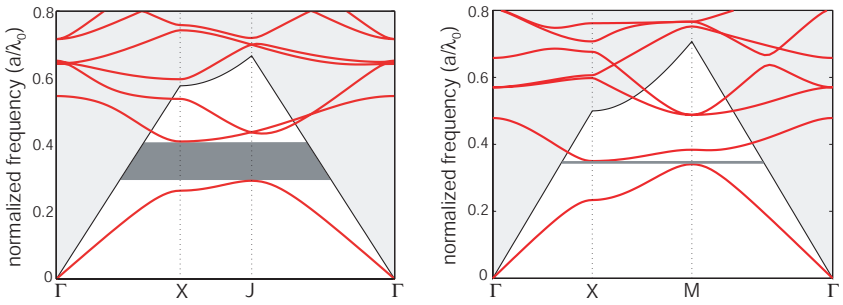

(a) Hexagonal Lattice in-plane bandstructure.

(b) Square Lattice in-plane bandstructure.

Fig. 4. Fundamental TE-like (even) guided mode bandstructure for hexagonal and square lattices, calculated using a 2D plane-wave expansion method with an effective index for the vertical guiding: (a) hexagonal lattice with $r/a = 0.36$, $n_{\text{slab}} = n_{\text{eff}} = 2.65$, (b) square lattice with $r/a = 0.40$, $n_{\text{slab}} = n_{\text{eff}} = 2.65$.

3.1 *Hexagonal Lattice*

For a hexagonal lattice, the high symmetry points about which a defect may be formed are points a (C_{6v} symmetry), b (C_{2v} symmetry), and c (C_{3v,σ_v} symmetry) shown in Figure 2(a). In this paper we consider donor and acceptor modes formed only at points a and b as from the analysis presented in reference [18] those centered at point c do not contribute modes with the requisite symmetry and dominant Fourier components. We also examine reduced symmetry modes formed at point a where the reduction of symmetry from C_{6v} to C_{2v} is accomplished by choosing a defect that breaks the symmetry of the lattice and is compatible with C_{2v}. Based upon the analysis of [13, 18], we create Table 1 for donor modes and Table 2 for acceptor modes. These tables provide the labeling scheme for the C_{6v} and C_{2v} modes, the dominant Fourier components of the modes, and their transformation properties about the available mirror planes (the mirror plane properties are represented by their character values[21]).

Donor modes of C_{6v} symmetry, formed at point a in the lattice, have their dominant Fourier components in the $\pm\{\mathbf{k}_{X_1}, \mathbf{k}_{X_2}, \mathbf{k}_{X_3}\}$ directions, and we thus require that $\sigma_d = -1$, where the σ_{d_i} are the mirror planes labeled in Figure 2(a). However, $\sigma_d \neq -1$ for the modes listed in Table 1. Reducing the symmetry of the mode to C_{2v} (through a modified defect at point a or re-centering to point b) results in modes with dominant Fourier components that are not orthogonal to the available mirror planes, or as in the case of the $\mathbf{B}_{B_1}^{b,d1}$ mode, incorrect spatial symmetry.

Out of the C_{6v} acceptor modes in Table 2, the $\mathbf{B}_{A_2''}^{a,a1}$ mode satisfies the symmetry criteria. The $\mathbf{B}_{A_2}^{b,a1}$ mode produced at position b does not quite satisfy our criteria, as two of the three pairs of dominant Fourier components ($\pm\{\mathbf{k}_{J_1}, \mathbf{k}_{J_3}\}$) are not orthogonal to the mirror planes; however, distortions of the lattice that preferentially select for the $\pm\mathbf{k}_{J_5}$ Fourier components over $\pm\mathbf{k}_{J_1}$ and $\pm\mathbf{k}_{J_3}$ can be made so that the symmetry condition is satisfied. Such lattice distortions are addressed in a future article. As a reference, the approximate form for the $\mathbf{B}_{A_2''}^{a,a1}$ mode is listed below [13]:

$$\mathbf{B}_{A_2''}^{a,a1} = \hat{z}\left(\cos(\mathbf{k}_{J_1}\cdot\mathbf{r}_{\perp}^{a}) + \cos(\mathbf{k}_{J_3}\cdot\mathbf{r}_{\perp}^{a}) + \cos(\mathbf{k}_{J_5}\cdot\mathbf{r}_{\perp}^{a})\right), \tag{1}$$

#1301 - $15.00 US
Received June 03, 2002; Revised July 17, 2002

where $\mathbf{r}_\perp^a$ denotes in-plane coordinates referenced to point a.

Table 1. Symmetry classification and dominant Fourier components for the **B**-field of conduction band donor modes in a hexagonal lattice.

defect center	C_{6v} modes	Fourier components	(σ_d, σ_v)[b]	C_{2v} modes	(σ_x, σ_y)[b]
$(0,0)$	$\mathbf{B}^{a,d1}_{B_1''}$	$\pm\{\mathbf{k}_{X_1}, \mathbf{k}_{X_2}, \mathbf{k}_{X_3}\}$	$(+,-)$	$\mathbf{B}^{a,d1,1}_{B_1}$	$(-,+)$
$(0,0)$	$\mathbf{B}^{a,d1}_{E_1,1}$	$\pm\{\mathbf{k}_{X_1}, \mathbf{k}_{X_2}, \mathbf{k}_{X_3}\}$	$(0,0)$	$\mathbf{B}^{a,d1,2}_{B_1}$	$(-,+)$
$(0,0)$	$\mathbf{B}^{a,d1}_{E_1,2}$	$\pm\{\mathbf{k}_{X_2}, \mathbf{k}_{X_3}\}$	$(0,0)$	$\mathbf{B}^{a,d1}_{B_2}$	$(+,-)$
$(a/2,0)$	N/A[a]	$\pm\{\mathbf{k}_{X_2}, \mathbf{k}_{X_3}\}$	N/A	$\mathbf{B}^{b,d1}_{A_1}$	$(+,+)$
$(a/2,0)$	N/A	$\pm\{\mathbf{k}_{X_2}, \mathbf{k}_{X_3}\}$	N/A	$\mathbf{B}^{b,d1}_{A_2}$	$(-,-)$
$(a/2,0)$	N/A	$\pm\{\mathbf{k}_{X_1}\}$	N/A	$\mathbf{B}^{b,d1}_{B_1}$	$(-,+)$

[a] Not Applicable. Modes centered at point b are of C_{2v} symmetry.
[b] Character values.

Table 2. Symmetry classification and dominant Fourier components for the **B**-field of valence band acceptor modes in a hexagonal lattice.

defect center	C_{6v} modes	Fourier components	(σ_d, σ_v)	C_{2v} modes	(σ_x, σ_y)
$(0,0)$	$\mathbf{B}^{a,a1}_{A_2''}$	$\pm\{\mathbf{k}_{J_1}, \mathbf{k}_{J_3}, \mathbf{k}_{J_5}\}$	$(-,-)$	$\mathbf{B}^{a,a1}_{A_2}$	$(-,-)$
$(0,0)$	$\mathbf{B}^{a,a1}_{B_2''}$	$\pm\{\mathbf{k}_{J_1}, \mathbf{k}_{J_3}, \mathbf{k}_{J_5}\}$	$(-,+)$	$\mathbf{B}^{a,a1}_{B_2}$	$(+,-)$
$(a/2,0)$	N/A	$\pm\{\mathbf{k}_{J_1}, \mathbf{k}_{J_3}, \mathbf{k}_{J_5}\}$	N/A	$\mathbf{B}^{b,a1}_{A_2}$	$(-,-)$
$(a/2,0)$	N/A	$\pm\{\mathbf{k}_{J_1}, \mathbf{k}_{J_3}, \mathbf{k}_{J_5}\}$	N/A	$\mathbf{B}^{b,a1}_{B_2}$	$(+,-)$

3.2 *Square Lattice*

The square lattice of air holes in a dielectric slab, whose real and reciprocal space representations are shown in Figure 2(b), and whose TE-mode bandstructure is depicted in Figure 4(b), also provides a photonic lattice from which low-loss defect modes can be formed. Defects in a square lattice may be centered at the C_{4v} symmetry points d and f, or the C_{2v} symmetry point e. Again, following the analysis of [18], we produce Tables 3 and 4 for the square lattice defect modes.

Based on their properties under mirror reflection, the $\mathbf{B}^{f,d1}_{A_2''}$, $\mathbf{B}^{f,d1}_{B_2''}$, and $\mathbf{B}^{e,d1}_{A2}$ donor modes all meet the symmetry condition we have placed on the modes. By suitable modification of the defect geometry, the symmetry of modes formed at points d and f can be reduced to C_{2v,σ_v} or C_{2v,σ_d}, where the subscript σ_v denotes symmetry with respect to the (σ_x,σ_y) mirror planes and the subscript σ_d refers to the ($\sigma_{x'}$,$\sigma_{y'}$) mirror planes (Figure 2(b)). The modes at f continue to satisfy the symmetry criteria under C_{2v,σ_v}, but no longer do so under C_{2v,σ_d}, as the σ_d mirror planes are not orthogonal to the modes' dominant Fourier components.

The acceptor states formed from the valence band edge at the M-point are analyzed in a similar fashion, and in this case, the modes at points d and f are candidates. The reduced symmetry C_{2v,σ_v} modes at points d and f are ruled out, while the C_{2v,σ_d} modes at these two high symmetry points remain on the list. As a reference, the approximate forms for the candidate donor and acceptor modes are given in Table 5 below.

#1301 - $15.00 US Received June 03, 2002; Revised July 17, 2002

Table 3. Symmetry classification and dominant Fourier components for the **B**-field of conduction band donor modes in a square lattice.

defect center	C_{4v} modes	Fourier comp.	(σ_d, σ_v)	C_{2v,σ_v} modes	(σ_x, σ_y)	C_{2v,σ_d} modes	$(\sigma_{x'}, \sigma_{y'})$
$(0,0)$	$\mathbf{B}^{d,d1}_{E,1}$	$\pm\{\mathbf{k}_{X_1}\}$	$(0,0)$	$\mathbf{B}^{d,d1}_{B_1}$	$(-,+)$	$\mathbf{B}^{d,d1}_{B'_1}$	$(-,-)$
$(0,0)$	$\mathbf{B}^{d,d1}_{E,2}$	$\pm\{\mathbf{k}_{X_2}\}$	$(0,0)$	$\mathbf{B}^{d,d1}_{B_2}$	$(+,-)$	$\mathbf{B}^{d,d1}_{B'_2}$	$(+,-)$
$(a/2,a/2)$	$\mathbf{B}^{f,d1}_{A''_2}$	$\pm\{\mathbf{k}_{X_1},\mathbf{k}_{X_2}\}$	$(-,-)$	$\mathbf{B}^{f,d1,1}_{A_2}$	$(-,-)$	$\mathbf{B}^{f,d1}_{A'_2}$	$(-,-)$
$(a/2,a/2)$	$\mathbf{B}^{f,d1}_{B''_2}$	$\pm\{\mathbf{k}_{X_1},\mathbf{k}_{X_2}\}$	$(-,+)$	$\mathbf{B}^{f,d1,2}_{A_2}$	$(-,-)$	$\mathbf{B}^{f,d1}_{A'_1}$	$(-,-)$
$(0,a/2)$	N/A	$\pm\{\mathbf{k}_{X_1}\}$	N/A	$\mathbf{B}^{e,d1}_{A2}$	$(-,-)$	N/A	N/A
$(0,a/2)$	N/A	$\pm\{\mathbf{k}_{X_2}\}$	N/A	$\mathbf{B}^{e,d1}_{B2}$	$(+,-)$	N/A	N/A

Table 4. Symmetry classification and dominant Fourier components for the **B**-field of valence band acceptor modes in a square lattice.

defect center	C_{4v} modes	Fourier comp.	(σ_d, σ_v)	C_{2v,σ_v} modes	(σ_x, σ_y)	C_{2v,σ_d} modes	$(\sigma_{x'}, \sigma_{y'})$
$(0,0)$	$\mathbf{B}^{d,a1}_{A''_2}$	$\pm\{\mathbf{k}_{M_1},\mathbf{k}_{M_2}\}$	$(-,-)$	$\mathbf{B}^{d,a1}_{A_2}$	$(-,-)$	$\mathbf{B}^{d,a1}_{A'_2}$	$(-,-)$
$(a/2,a/2)$	$\mathbf{B}^{f,a1}_{B''_1}$	$\pm\{\mathbf{k}_{M_1},\mathbf{k}_{M_2}\}$	$(+,-)$	$\mathbf{B}^{f,a1}_{A_1}$	$(+,+)$	$\mathbf{B}^{f,a1}_{A'_2}$	$(-,-)$
$(0,a/2)$	N/A	$\pm\{\mathbf{k}_{M_1},\mathbf{k}_{M_2}\}$	N/A	$\mathbf{B}^{e,a1}_{B_1}$	$(-,+)$	N/A	N/A

Table 5. Candidate donor and acceptor modes in a square lattice.

Donor Modes	**Acceptor Modes**
$\mathbf{B}^{f,d1}_{A''_2} = \hat{z}\big(\cos(\mathbf{k}_{X_1}\cdot\mathbf{r}^f_\perp) + \cos(\mathbf{k}_{X_2}\cdot\mathbf{r}^f_\perp)\big)$	$\mathbf{B}^{d,a1}_{A''_2} = \hat{z}\big(\cos(\mathbf{k}_{M_1}\cdot\mathbf{r}^d_\perp) + \cos(\mathbf{k}_{M_2}\cdot\mathbf{r}^d_\perp)\big)$
$\mathbf{B}^{f,d1}_{B''_2} = \hat{z}\big(\cos(\mathbf{k}_{X_1}\cdot\mathbf{r}^f_\perp) - \cos(\mathbf{k}_{X_2}\cdot\mathbf{r}^f_\perp)\big)$	$\mathbf{B}^{f,a1}_{B''_1} = \hat{z}\big(\cos(\mathbf{k}_{M_1}\cdot\mathbf{r}^f_\perp) - \cos(\mathbf{k}_{M_2}\cdot\mathbf{r}^f_\perp)\big)$
$\mathbf{B}^{e,d1}_{A2} = \hat{z}\big(\cos(\mathbf{k}_{X_1}\cdot\mathbf{r}^e_\perp)\big)$	

4 Initial FDTD Simulation Results

The symmetry analysis presented in the previous section determined the modes satisfying our symmetry criteria, chosen to reduce vertical radiation losses from the PC slab WG. For a hexagonal lattice, we singled out the acceptor mode of equation 1, while for the square lattice, a number of options were available, as summarized in Table 5. We begin the 3D FDTD analysis of high-Q PC resonant cavities by choosing particular defects in the hexagonal and square lattices that will support one of these modes. Results from the FDTD analysis will provide a measure of the benefits obtained in using modes of such symmetries, and will also give an indication of what further improvements are needed. This will lead naturally to the Fourier space tailoring of the lattice discussed in Section **5**.

The FDTD calculations presented in this section were performed on a mesh with 20 points per lattice spacing (greater than 70 points per free space wavelength or 20 points

#1301 - $15.00 US Received June 03, 2002; Revised July 17, 2002

per wavelength in the dielectric). Cavity modes were excited by an initial field (B_z) with a localized Gaussian profile, and even modes of the slab WG were preferentially selected by using an even mirror symmetry condition ($\sigma_h = 1$) in the middle of the slab. In order to maintain a single vertical mode of the PC slab waveguide (within the frequency band of interest), we choose a normalized slab thickness $d/a = 0.75$ in this section. Where appropriate, the mirror planes (σ_x, σ_y) were used to filter out cavity modes according to their projection on to the irreducible representations (IRREPs) of C_{2v,σ_v}. Mur's absorbing boundary conditions were used to terminate the FDTD simulation domain in all other directions. Q values were calculated by determining the power absorbed in the boundaries (P_{abs}) and the stored energy in the mode (U), and taking $Q = \omega_0 U/P_{abs}$, where ω_0 was the angular frequency of the mode. By distinguishing between power flow to vertical and in-plane boundaries, effective Q values $Q_\perp$ and $Q_\parallel$ were calculated. It should be noted that a number of other methods were also used to estimate the Q values, including the modal energy decay rate and the radiated power calculated from the near-field momentum components lying within the cladding light cone, all resulting in consistent values. The effective volume of the cavity modes, V_{eff} in the tables below, is calculated here using the peak in the electric field energy density and is given in units of cubic half-wavelengths in vacuum[15]. Further details on the simulation methods can be found in previous articles [13, 15, 16].

4.1 *Hexagonal Lattice*

The $\mathbf{B}_{A_2''}^{a,a1}$ mode, our candidate mode for study, is formed by enlarging holes in a manner consistent with the C_{6v} symmetry of the lattice, so that an acceptor mode is formed. We choose the defect geometry shown in Table 6, where the central hole (about point a) is enlarged from radius r to r'. The defect is surrounded by a total of 8 periods of the hexagonal lattice in the $\hat{x}$-direction and 12 periods in the $\hat{y}$-direction. The magnetic field amplitude and momentum space electric field components $\widetilde{\mathbf{E}}_x$ and $\widetilde{\mathbf{E}}_y$ of mode $\mathbf{B}_{A_2''}^{a,a1}$ are given in Table 6 for two different pairs of values (r, r'). The dominant Fourier components are seen to be $\pm\{\mathbf{k}_{J_1}, \mathbf{k}_{J_3}, \mathbf{k}_{J_5}\}$, as predicted by the symmetry analysis. Examining $\widetilde{\mathbf{E}}_x$ and $\widetilde{\mathbf{E}}_y$, it is also clear that, although the power within the light cone has been reduced in comparison to the x-dipole donor mode, it is still significant. This fact is evidenced in $Q_\perp$ which, at $4,900$ for $r/a = 0.35$ and $r'/a = 0.45$, is larger than that obtained for the x-dipole mode. By reducing the frequency, and consequently the radius of the light cone, the PC cavity with $r/a = 0.30$ and $r'/a = 0.45$ has an improved vertical Q of $8,800$ (although its in-plane Q has degraded due to a reduction in the in-plane bandgap for smaller lattice hole radii).

One complication in the hexagonal lattice (as opposed to the square lattice designs studied below) is the number of dominant Fourier components that must be accounted for when trying to maximize Q. As we alluded to earlier, modifications to the host lattice itself, rather than the defect geometry alone, provide an interesting method to reduce the number of components and further improve the Q of the structure. The detailed discussion of these ideas is left to an upcoming paper. From this point on, we will focus on square lattice designs, but it is important to note that many of the ideas described below are equally applicable to hexagonal lattice structures.

4.2 *Square Lattice*

We choose the $\mathbf{B}_{A2}^{e,d1}$ mode as our candidate for study. This mode, centered in the dielectric at point e in the lattice, is appealing in that it has Fourier components primarily situated at $\pm\mathbf{k}_{X_1}$, while the other modes of correct symmetry have a larger number of Fourier components. This simplifies the design considerations of Section **5**. To create

#1301 - $15.00 US Received June 03, 2002; Revised July 17, 2002

Table 6. Characteristics of the $\mathbf{B}_{A_2''}^{a,a1}$ resonant mode in a hexagonal lattice (images are for a PC cavity with $r/a = 0.35$, $r'/a = 0.45$, $d/a = 0.75$, and $n_{\text{slab}} = 3.4$).

Geometry	$\lvert\mathbf{B}\rvert$	$\lvert\widetilde{\mathbf{E}}_x\rvert$	$\lvert\widetilde{\mathbf{E}}_y\rvert$
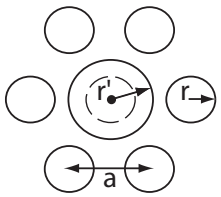	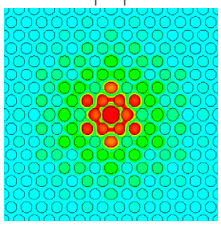	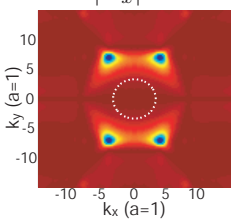	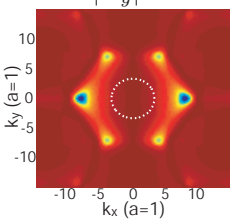

$\mathbf{r}/\mathbf{a}$	$\mathbf{r}'/\mathbf{a}$	$\omega_n = a/\lambda_o$	$\mathbf{Q}_{\parallel}$	$\mathbf{Q}_{\perp}$	$\mathbf{Q}_{\text{tot}}$	$\mathbf{V}_{\text{eff}}$
0.35	0.45	0.265	34,100	4,900	4,300	0.11
0.30	0.45	0.248	5,300	8,800	3,300	0.17

the mode, we consider the structure depicted in Table 7. Defining point e as the origin, $(0, 0)$, we see that the structure consists of a standard square lattice of air holes in which the two holes centered at $(0, \pm a/2)$ are decreased in size so as to create a donor mode of A_2 symmetry. In the FDTD simulations, the structure consists of 12 rows and 8 columns of air holes surrounding the defect holes.

Starting with $r/a = 0.30$, $r'/a = 0.28$, and $d/a = 0.75$, we produce a mode with normalized frequency $\omega_n = a/\lambda_o = 0.264$. The magnetic field amplitude and 2D spatial FTs ($\widetilde{\mathbf{E}}_x$ and $\widetilde{\mathbf{E}}_y$) of the mode are given in Table 7. As the magnitude of $\widetilde{\mathbf{E}}_y$ is negligible in comparison to that of $\widetilde{\mathbf{E}}_x$, the mode is predominantly made up of components centered at $\pm\mathbf{k}_{X_1}$, as predicted. The effective vertical Q of this mode is approximately $54,000$, easily exceeding the values obtained in [13] for a mode of even symmetry. The small $Q_{\parallel}$ $(17,400)$ is a result of the weak defect perturbation and extended nature of the cavity mode ($V_{\text{eff}} = 0.43$). Improving the localization of the mode by lowering r'/a of the defect to 0.25 improves $Q_{\parallel}$ to a value of $60,000$ and lowers V_{eff} by a factor of almost two. Surprisingly, $Q_{\perp}$ has also increased from $54,000$ to $69,000$ despite the stronger localization of the mode and its expected broadening in Fourier space. This rather counter-intuitive result indicates that a more detailed study of the effects of the defect geometry on cavity loss is required. This is the focus of the following section.

5 Momentum Space Design of the Defect Geometry in a Square Lattice

The results given thus far indicate that improving the loss properties of the defect mode resonators requires isolation of the mode's momentum components to regions outside the light cone to maintain a high $Q_{\perp}$, and to those regions for which the in-plane bandgap is substantial for a high $Q_{\parallel}$. To determine how to tailor the defect geometries to accomplish these goals, we consider a simple model to illustrate the couplings induced in Fourier space between the dominant momentum components of a given defect mode and those modes which radiate. We employ a two-step process where in the first step, the approximate form of the defect mode is taken based on symmetry arguments, as outlined in Section **3**, with the allowance for finite **k**-space bandwidths in the dominant Fourier components due to the localization of the defect mode. We then consider couplings of this approximate symmetry mode to other modes of the PC slab WG through the dielectric perturbation $\Delta\eta(\mathbf{r})$, where $\eta = 1/\epsilon$ is the inverse of the dielectric profile of the lattice. The most important mode couplings from the perspective of increasing the

#1301 - $15.00 US
Received June 03, 2002; Revised July 17, 2002

Table 7. Characteristics of the $\mathbf{B}_{A2}^{e,d1}$ resonant mode in a square lattice (images are for a PC cavity with $r/a = 0.30$, $r'/a = 0.28$, $d/a = 0.75$, and $n_{\text{slab}} = 3.4$).

Geometry	$\lvert\mathbf{B}\rvert$	$\lvert\widetilde{\mathbf{E}}_x\rvert$	$\lvert\widetilde{\mathbf{E}}_y\rvert$
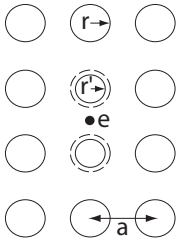	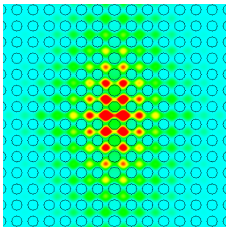	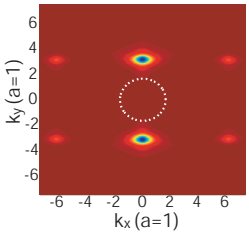	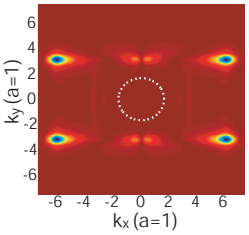

$\mathbf{r}/\mathbf{a}$	$\mathbf{r}'/\mathbf{a}$	ω_n	$\mathbf{Q}_{\parallel}$	$\mathbf{Q}_{\perp}$	$\mathbf{Q}_{\text{tot}}$	$\mathbf{V}_{\text{eff}}$
0.30	0.28	0.265	17,400	54,000	13,000	0.43
0.30	0.25	0.262	60,100	69,200	32,000	0.22

Q are those between the dominant Fourier components and "leaky cavity modes". The leaky cavity modes consist of vertical radiation modes and guided modes of the PC slab WG which are not reflected by the PC and thus leak in-plane. $\Delta\eta$ induces the change $\delta\mathbf{H}^d(\mathbf{r})$ in the defect mode, and this change is written as a superposition over the set of nearly (frequency) degenerate guided and radiation modes of the PC slab WG. The coupling amplitude between the symmetry mode composed of the dominant Fourier components, $\mathbf{H}_o^d(\mathbf{r})$, and a leaky cavity mode, $\mathbf{H}_o^{lcm}(\mathbf{r})$, of the unperturbed PC slab is given by the following matrix element:

$$\int d^3r \left(\mathbf{H}_o^{lcm}(\mathbf{r})\right)^* \left(\nabla\times\left(\Delta\eta(\mathbf{r})\nabla\times\mathbf{H}_o^d(\mathbf{r})\right)\right) \sim \int \frac{d^2k_\perp}{(2\pi)^4}\left(\widetilde{B}_{z,o}^{lcm}\right)^* \left(\left[\widetilde{\Delta\eta} * \left(|\mathbf{k}_\perp|^2 \widetilde{B}_{z,o}^d\right)\right] + \left[\left(k_x\widetilde{\Delta\eta}\right) * \left(k_x\widetilde{B}_{z,o}^d\right)\right] + \left[\left(k_y\widetilde{\Delta\eta}\right) * \left(k_y\widetilde{B}_{z,o}^d\right)\right]\right) \quad (2)$$

where $*$ denotes convolution. In converting from the real space integral to momentum space, we have neglected the variation of $\eta(\mathbf{r})$ and $\Delta\eta(\mathbf{r})$ in the $\hat{z}$-direction, so that $\mathbf{H}_o^d(\mathbf{r}) \approx {B_{z,o}}^d(\mathbf{r}_\perp)$ (TE-like mode). From this equation, it is clear that the FT of the dielectric perturbation, $\widetilde{\Delta\eta}(\mathbf{k}_\perp)$, is the key quantity that couples Fourier components between the basis modes of the system. By tailoring this quantity appropriately, we can thus limit couplings that lead to in-plane and vertical leakage. Such a tailoring can be implemented for both the square and hexagonal lattice designs; however, due to the relative simplicity of the Fourier space representation of the $\mathbf{B}_{A2}^{e,d1}$ defect mode in the square lattice, we focus on it in this paper. The implementation of Fourier space design rules in standard and distorted hexagonal lattices is discussed in future work.

Our candidate mode, $\mathbf{B}_{A2}^{e,d1}$, has dominant in-plane Fourier components at $\pm\mathbf{k}_{X_1}$. We must therefore modify the defect so that $\widetilde{\Delta\eta}$ does not couple the $\pm\mathbf{k}_{X_1}$ momentum components to those regions in $\mathbf{k}$-space which are "leaky". In order to reduce radiation normal to the PC slab through coupling to the light cone, the amplitude of $\widetilde{\Delta\eta}$ in the neighborhood of $k_y = \pm\pi/a$ should be minimized. In addition, for the square lattice designs investigated here the bandgap between the conduction band-edge at the X-point and the valence band-edge at the M-point is at best very narrow, consequently, we look to reduce coupling between neighborhoods surrounding the X- and M-points.

#1301 - $15.00 US
Received June 03, 2002; Revised July 17, 2002

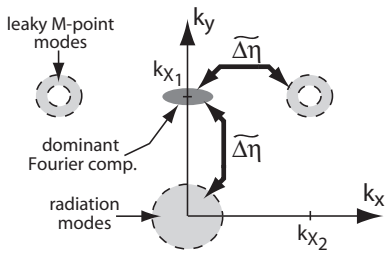

Fig. 5. Illustration showing the mode coupling for the $\mathbf{B}_{A2}^{e,d1}$ mode in $\mathbf{k}$-space through the $\widetilde{\Delta\eta}$ perturbation.

This implies that it will also be necessary to reduce the amplitude of $\widetilde{\Delta\eta}$ in the region about $k_x = \pm\pi/a$.

The crux of the argument described above is depicted in Figure 5, where lossy couplings are illustrated for the upper region of $\mathbf{k}$-space (the negative k_y region will behave identically in this case). Here we have assumed that the defect mode frequency lies below the conduction band-edge at the X-point but slightly within the valence band near the M-point, resulting in an annular region of $\mathbf{k}$-space about the M-point which is strongly coupled to. With reference to this simple schematic, the Fourier components of $\widetilde{\Delta\eta}$ that lead to radiation losses from the defect cavity are approximately:

$$\begin{aligned}
&\widetilde{\Delta\eta}\Big(|k_x| \lesssim (k_{\rm lc} + \Delta_x),\, |k_y \pm |\mathbf{k}_{X_1}|| \lesssim (k_{\rm lc} + \Delta_y)\Big) \Longrightarrow \text{coupling to light cone,} \\
&\widetilde{\Delta\eta}\Big(|k_x \pm |\mathbf{k}_{X_2}|| \lesssim \Delta_x,\, |k_y| \lesssim \Delta_y\Big) \Longrightarrow \text{coupling to leaky } M\text{-point.}
\end{aligned} \tag{3}$$

where k_{lc} is the radius of the light cone, and Δ_x and Δ_y are the widths of the dominant Fourier peaks in the $\widehat{k}_x$- and $\widehat{k}_y$-directions, respectively.

Before attempting any design modifications, we first consider the simple defect geometry studied in Section **4**, where the holes located at $(0, \pm a/2)$ were reduced from the standard hole radius r to a radius r'. The perturbation $\Delta\eta$ is given by the difference in η with and without the defect holes, and thus simply consists of a pair of annuli, each of width $(r - r')$, centered at $(0, \pm a/2)$. The 2D spatial FT of this function can be obtained analytically[22], and is separable into the form

$$\widetilde{\Delta\eta}(\mathbf{k}_\perp) = F(k_\perp; r, r') \cos\left(\frac{k_y a}{2}\right), \tag{4}$$

where $F(k_\perp; r, r')$ is a function of the magnitude of the in-plane momentum, with r and r' as parameters. This function, along with one-dimensional (1D) slices along the k_x and k_y axes, is shown in figure 6 (the figure shown is actually the direct FT of the structure used in FDTD calculations, to take into account any staircasing effects in the rendering of the holes; however, the difference between it and the analytic function are insignificant.). We notice, as is clear from examining eq. (4), that $\widetilde{\Delta\eta} = 0$ at $k_y = \pm\pi/a$. Our choice of defect was thus a fortuitous one, as the zero amplitude of $\widetilde{\Delta\eta}$ at the X points eliminated coupling between the dominant Fourier components of the $\mathbf{B}_{A2}^{e,d1}$ mode and DC. Of course, a localized defect mode has a finite bandwidth in Fourier space about its dominant momentum components, and the light cone encompassing the radiation modes is of finite radius as well. As a result it is desirable to minimize the Fourier components of the dielectric perturbation over an extended region about $k_y = \pm\pi/a$.

#1301 - $15.00 US
Received June 03, 2002; Revised July 17, 2002

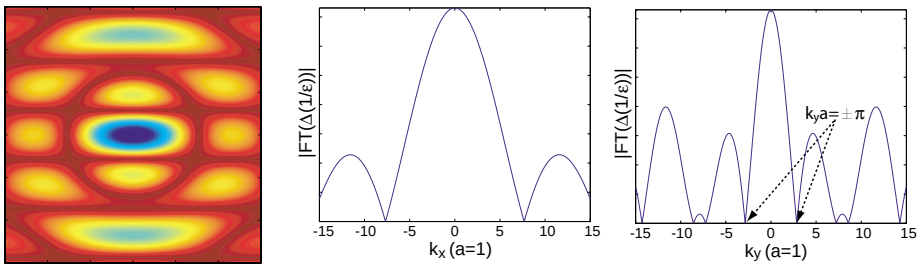

(a) 2D. (b) Along k_x axis. (c) Along k_y axis.

Fig. 6. $\widetilde{\Delta\eta}(\mathbf{k}_\perp)$ for dielectric structure of Table 7.

Note that $\widetilde{\Delta\eta}$ for the hexagonal lattice design of the previous section does not have zero amplitude at any of the $\mathbf{k}_J$, and thus the $Q_\perp$ values are much smaller than those of the square lattice. To increase $Q_\perp$ in the hexagonal lattice, future designs must therefore tailor the lattice in a way so that this amplitude is significantly reduced.

It is also necessary to modify the dielectric to improve $Q_\parallel$. The most straightforward way to immediately do so is to increase the r/a of the host PC, as that will provide a bandgap for an increased range of momentum values. This also tends to decrease $Q_\perp$, as the increased r/a will produce a mode of higher frequency, resulting in a cladding light cone of increased radius encompassing a larger range of momentum values. Fortunately, this does not necessarily have to hold for a general defect geometry. In particular, the hole radius can be kept relatively small in the region where the mode is primarily located, but can be graded outside this region to increase the in-plane reflectivity. The choice of grading can be determined by considering the need to limit the in-plane momentum components of the mode to regions in which the bandgap is substantial (Note that for the simple two-hole design considered in Section **4**, $\widetilde{\Delta\eta}$ is quite large in this region of momentum space about $k_x = \pm\pi/a$). The benefit of this approach is that it does not necessarily result in increased vertical radiation loss, thus allowing for both a large $Q_\parallel$ and $Q_\perp$.

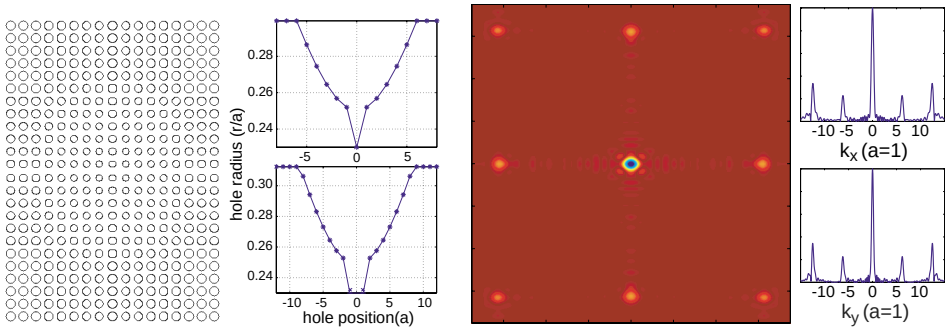

(a) Graded PC lattice. (top right) r/a along y=a/2. (bottom right) r/a along x=0.

(b) $\widetilde{\Delta\eta}(\mathbf{k}_\perp)$. (top right) $\widetilde{\Delta\eta}(\mathbf{k}_\perp)$ along k_x axis. (bottom right) $\widetilde{\Delta\eta}(\mathbf{k}_\perp)$ along k_y axis.

Fig. 7. Properties of the graded square lattice.

#1301 - $15.00 US
Received June 03, 2002; Revised July 17, 2002

Consider the graded lattice shown in figure 7(a). The standard defect holes at $(0, \pm a/2)$ have $r/a = 0.23$, while their immediate neighbors have $r/a = 0.253$. The hole radii are then increased parabolically outwards for 5 periods in the $\hat{x}$-direction and 7 periods in the $\hat{y}$-direction, after which they are held constant. The nature of this grading is shown in figure 7(a), where the r/a profiles are given for slices along $y = a/2$ and $x = 0$. Along these axes the maximum value r/a attains is 0.31, but along the diagonal directions r/a grows to be as large as 0.35. The dielectric perturbation, which now consists of a series of annuli of decreasing width from the center to the edges, has a FT given in Figure 7(b). Examining both the 2D image and the 1D line scans of the FT, we see that our grading has greatly diminished the amplitude of $\widetilde{\Delta\eta}$ in the regions surrounding $k_y = \pm\pi/a$ and $k_x = \pm\pi/a$.

The FDTD simulations of the defect mode of this structure largely confirm the ideas described thus far. $Q_\perp$ has increased to over $110,000$, while $Q_\parallel$ has improved even further to approximately $470,000$, giving an overall $Q_{\text{tot}} \approx 89,000$. The magnetic field amplitude and FT of the in-plane electric field components in Table 8 support these results. In particular, consider the line scan of $\widetilde{\mathbf{E}}_x$ along the k_y axis. It shows that the grading has met with success, as power has largely been eliminated within the light cone. This point is particularly striking when contrasted with the corresponding image shown in Figure 3(b) for the low Q x-dipole mode we took as our baseline. Note that $\widetilde{\Delta\eta}(k_x = 0, k_y = \pm\pi/a)$ is identically zero regardless of the grade, due to the position of the defect holes with respect to the center of the defect, whereas $\widetilde{\Delta\eta}(k_x = \pm\pi/a, k_y = 0)$ is not automatically zero. It may be advantageous to identically zero $\widetilde{\Delta\eta}(k_x = \pm\pi/a, k_y = 0)$ as this will allow for the formation of a more localized mode that is still of high $Q_\parallel$. Such a mode would be centered at the f-point of the square lattice, and would either be the $\mathbf{B}^{f,d1}_{A_2''}$ or $\mathbf{B}^{f,d1}_{B_2''}$ mode.

Table 8. Field characteristics of graded square lattice shown in figure 7(a).

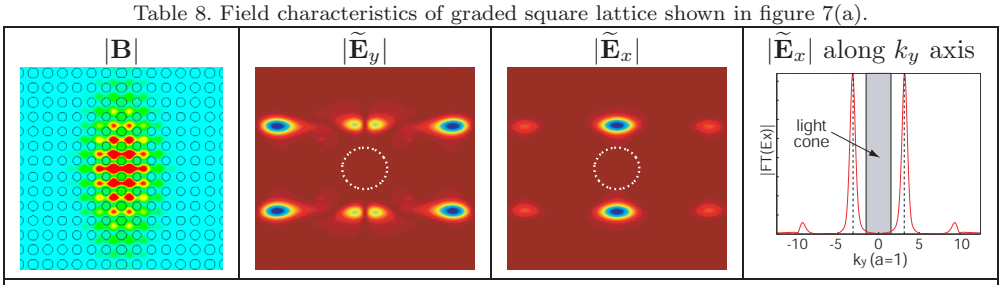

d/a	ω_n	$\mathbf{Q}_\parallel$	$\mathbf{Q}_\perp$	$\mathbf{Q}_{\text{tot}}$	$\mathbf{V}_{\text{eff}}$
0.75	0.245	470,000	110,000	89,000	0.25
0.85	0.239	422,000	128,000	98,000	0.26
0.95	0.235	296,000	139,000	95,000	0.27
1.05	0.231	280,000	145,000	96,000	0.28

Before concluding, there are a couple of points concerning the chosen lattice that are worth mentioning. The first is that the initial jump in r/a between the defects at $(0, \pm a/2)$ and their neighbors is an important element of this design. Acting as a potential well, the jump helps confine the mode in real space, allowing r/a to increase quickly to a value for which the in-plane reflectivity is high without significantly increasing the modal frequency. The size of the jump is also important; if incorrectly sized the resulting dielectric perturbation contains larger Fourier amplitudes which couple the mode to the

#1301 - $15.00 US
Received June 03, 2002; Revised July 17, 2002

M-point for which the PC is no longer reflective and to the light cone in which light radiates vertically. Simulations have been run on similar structures that do not have an initial jump, but rather are smoothly graded from $r/a = 0.23 - 0.35$. The performance significantly degrades in such a design, with $Q_\perp$ and $Q_\parallel$ dropping to $62,000$ and $9,700$, respectively. A similar Q-degradation is observed for gradings which occur too quickly, as a result of the stronger mode localization and subsequent Fourier space broadening of the mode. An optimum defect design is found when a compromise is struck between the minimization of the Fourier components of $\widetilde{\Delta\eta}$ which couple the dominant momentum components of the defect mode to regions of $\mathbf{k}$-space which radiate, and the degree to which the dominant momentum components of the mode broaden due to in-plane confinement by the defect.

It should again be emphasized that the increased $Q_\perp$ for these graded lattice designs is not solely the result of real-space delocalization of the mode. It is instead largely due to the aforementioned reduction of amplitude for those Fourier components of the dielectric perturbation that couple the dominant momentum components of the defect mode to those which radiate. Of course, real-space localization plays a role in determining the spread in $\mathbf{k}$-space of the dominant Fourier components of the mode, and if this spread exceeds the size of the region about $\pm\mathbf{k}_{X_1}$ that $\widetilde{\Delta\eta}$ has been flattened, vertical radiation will result. An increase in the slab thickness also effects the performance of the structure. It causes a decrease in the frequency of the mode, thus increasing $Q_\perp$. It also slightly reduces the size of the in-plane bandgap, decreasing $Q_\parallel$. This is in fact seen in the results of FDTD simulations compiled in Table 8.

Finally, we note that the criteria for choosing the geometries presented in this paper were entirely based on Q considerations, and optimization of the lattice grading to further increase Q can still be made. Changes may also be made to improve other aspects of the design. In particular, reducing the mode volume may be of importance to applications in quantum optics, while reducing the complexity of the design (in terms of the number and size of holes comprising the defect) may be of interest from a fabrication standpoint. The approach to such designs can be aided through the Fourier space consideration of the dielectric perturbation as has been described in this section. Doing so will elucidate the potential lossy couplings that occur when the defect mode is formed, and will help determine whether a given structure is able to sustain a high-Q mode.

6 Summary

The design of high-Q defect modes in a 2D PC slab WG has been developed through use of momentum space methods. Starting with the fundamental criterion that the reduction of vertical radiation losses requires an elimination of momentum components within the light cone of the slab waveguide, we proceed to present methods by which this is accomplished. The first is through a judicious choice of the mode's symmetry so that it is odd about mirror planes orthogonal to the mode's dominant Fourier components. To determine the precise nature of the symmetry for such modes in square and hexagonal lattices, we refer to the symmetry analysis of [13, 18], from which we produce a set of candidate modes that satisfy this momentum space criteria. Although symmetry alone can reduce vertical radiation loss, further modifications of the defect geometry based upon Fourier space considerations can be used to increase Q even further. Tailoring the lattice to avoid momentum space couplings which lead to in-plane and vertical radiation losses, we present graded square lattice structures for which $Q_\perp$ exceeds 10^5 while maintaining $Q_\parallel$ in the $3-5\times10^5$ range, demonstrating the possibility of producing high-Q modes in a planar PC slab WG by using these techniques.

K. Srinivasan thanks the Hertz Foundation for its financial support.

#1301 - $15.00 US Received June 03, 2002; Revised July 17, 2002